Real-Time Simulation of Level 1, Level 2, and Level 3 Electric Vehicle Charging Systems

Li Bao, Lingling Fan*, Zhixin Miao

*Department of Electrical Engineering, University of South Florida, Tampa FL USA 33620.

Email: linglingfan@usf.edu.

Abstract

A charging system is required to convert ac electricity from the grid to dc electricity to charge an electric vehicle (EV) battery. According to the Society of Automatic Engineers (SAE) standard, EV chargers can be divided into three levels based on power rating: Level 1, Level 2, and Level 3. This paper investigates the circuit topologies and control principles of EV charging systems at each level. Three high-fidelity testbeds of EV charging systems for a 10 kWh battery are designed and implemented in real-time digital simulator RT-Lab. The testbeds include modeling details such as switching of semiconductors. Twenty-five minutes real-time simulation is conducted for each testbed. Detailed dynamic performance of the circuits and the controls at every stage are presented to demonstrate the charging process. All three level EV charging systems employ high-frequency transformer embedded dual active bridge (DAB) dc/dc converter to regulate battery side dc voltage and current. Hence, average model-based linear system analysis is given to configure the parameters of the phase shift control adopted by the DAB dc/dc converter. In addition, power factor control (PFC) that is employed for Level 1 and Level 2 single-phase ac charging systems, three-phase voltage source converter control that is employed for Level 3 three-phase ac charging systems, are all analyzed. The three testbeds, with their detailed circuit parameters and control parameters presented, can be used as reference testbeds for EV grid integration research.

Keywords: Battery charging, RT-Lab, real-time simulation

1. Introduction

Environmental degradation, energy security and oil depletion urge governments and society to use clean energy. In U.S., the transportation energy consumption accounted for 29% of total energy in 2017 [1]. Majority of the energy consumed is fossil oil. The large amount consumption of oil causes air pollution by carbon dioxide emission, nitrogen oxide emission and other poisonous gases. Therefore, the traditional transportation vehicles, such as internal combustion engine vehicles, are expected to be reduced, while EVs are expected to have increased usage.

EVs use electrical power stored in a battery to drive motors. The battery is charged from grid through a charging system that converts the grid ac electricity to dc electricity. The charging system is categorized into three levels according the SAE standard [2]. Level 1 charger utilizes household outlets for overnight charging. The charging voltage is consistent with house use at 120 V level. The charging time is about 12 hours. Level 1 charging is the slowest charging. Level 2 charger is designed for private or public facilities

such as workplace or mall. The charging voltage is 240 V and the current is up to 60 A. Level 3 charging is fast charging for commercial use. Level 3 chargers are located at specific locations. Level 3 chargers use three phase voltage sources and have over 20 kW power level. The three charging levels are summarized in Table 1.

Table 1: Charging levels summarization

Charging Level	Supply Voltage	Charging Current	Rating Power
Level 1	120 V, single-phase	up to 16 A	up to 1.92 kW
Level 2	240 V, single-phase	up to 60 A	up to 14.4 kW
Level 3	Not finalized, 3-phase	Not finalized	over 20 kW

In order to realize high efficiency in power transfer and convert AC grid voltage to DC voltage, a charging system may include a rectifier to rectify ac to dc, a power factor correction (PFC) boost dc-dc circuit to achieve unity power factor, and a dual-active-bridge (DAB) dc-dc converter to achieve flexible dc to dc voltage conversion. The controls include DC bus voltage control, PFC control and constant current/constant voltage (CC/CV) control.

Computer simulation is the cheapest tool to conduct experiments. Considering the complicated model and control structure, the off-line simulation software such as PSCAD and PSpice become ill suited due to low simulation speed and limited memory. Compared to the off-line simulation, real-time simulation is able to provide fast, reliable and accurate simulation [3].

In this paper, three testbeds representing three levels of EV charging systems will be implemented in Real-Time Laboratory (RT-Lab), a real-time simulator developed by Opal-RT technologies [4, 5, 6].

The paper investigates the detailed models of charging systems, including their circuit topologies and control structures. Principles of each control, e.g., PFC, phase shift, are examined in detail. The models are then implemented in RT-Lab. Simulation results such as the inductor current of PFC, DC bus voltage, phase shift of DAB's ac voltage at two ends, and battery state-of-charge (SOC) are presented and examined. The three testbeds are compared for 25 minutes' real-time simulation of 10 kWh battery charging. To the authors best knowledge, there is no existence of real-time simulation models for EV chargers of all three level in the literature.

The contribution of this paper is two-fold. (1) Simulation models of EV charging systems at three levels are developed in RT-Lab real-time simulator in discrete time domain. (2) The charging process and the principles of control strategies are examined and further validated through real-time simulation results.

The rest of the paper is organized as follows. Level 1 and Level 2 charging systems are presented in Section 2. Level 3 charging system is presented in Section 3. The RT-Lab structure and performance are illustrated in Section 4. Section 5 demonstrates the real-time simulation results for the three testbeds. Finally Section 6 concludes this paper.

2. Level 1 and Level 2 charging systems

Both Level 1 and Level 2 charging systems use single phase ac voltage as source. The ac electricity firstly is passed to the diode-based AC/DC converter and is rectified to a DC form. A PFC boost circuit is followed

to adjust the DC voltage and improve the power factor. A bidirectional DAB converter is used to convert dc voltage from one level to another level. The CC/CV control is realized by the DAB converter control. A high frequency transformer is embedded in the DAB for the galvanic isolation and to boost voltage. A typical Level 1 or Level 2 charging circuit topology is shown in Fig. 1 as indicated in [7]. The battery model, PFC and DAB control will be described and analyzed as follows.

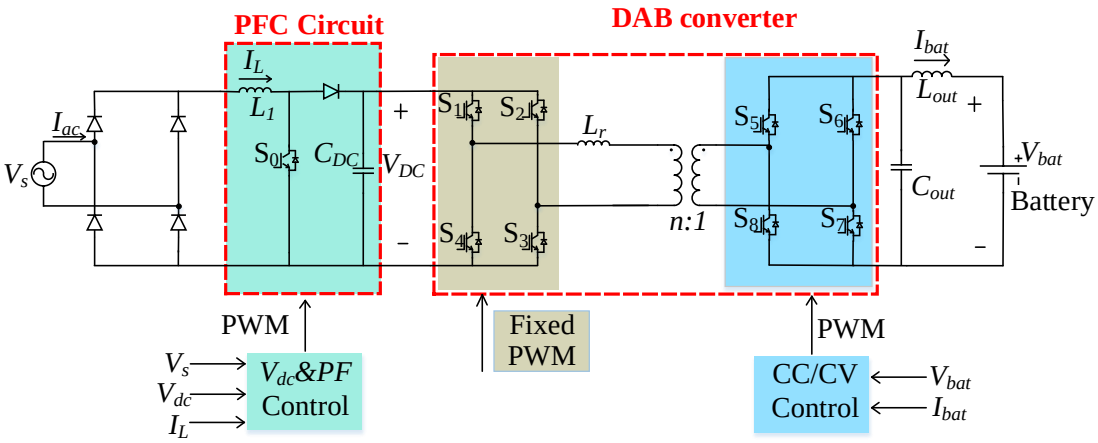

Figure 1: Topology of a Level 1 or Level 2 charging system. $f_{PWM} = 2\ kHz$, $L_{out} = 95\ mH$, $C_{out} = 0.1\ mF$, $n = 1$. For Level 1 model, $L_r = 1\ mH$, $V_s = 120\ V$ RMS. For Level 2 model, $L_r = 0.13\ mH$, $V_s = 240\ V$ RMS.

2.1. Battery model and charging control

Battery is a key part in the EVs. The size of the battery determines the driving ranging and charging time of the EVs. The battery stores chemical energy that converted from electricity and releases electricity power to supply EVs working.

Currently, the lithium-ion battery is the most common and has been popularly used. Compared to other types batteries, e.g., nickel-zinc or Ni-Cd battery, lithium-ion battery offers lighter weight and higher power density. The capacity of a battery is measured as ampere-hours (Ah). The stored energy is measured in watt-hours (Wh). The SOC is used to represent the current energy available in battery. SOC for a fully charge battery is 100% and 0% for fully discharged.

Assuming the battery terminal voltage is constant, the SOC can be defined as:

$$SOC = 100 \times (1 - \frac{1}{C}\int_0^t i(t)dt) \tag{1}$$

where C is battery capacity, $i(t)$ is battery terminal current.

In this paper, Matlab/SimPowerSystems' battery model is used. Fig. 2 illustrates the charging and discharging process of a battery [8]. A fully charged battery starts to discharge at full voltage. Then the voltage will keep an almost stationary value at the nominal area. This area releases most of stored energy. At the last region, the voltage drops rapidly.

The charging process is one of the most critical factors in battery application. Inappropriate charging method may shorten battery life and even damage battery through overheating or overcharging. Based on [9], there are three types of charging methods: constant current (CC), constant voltage (CV), and taper

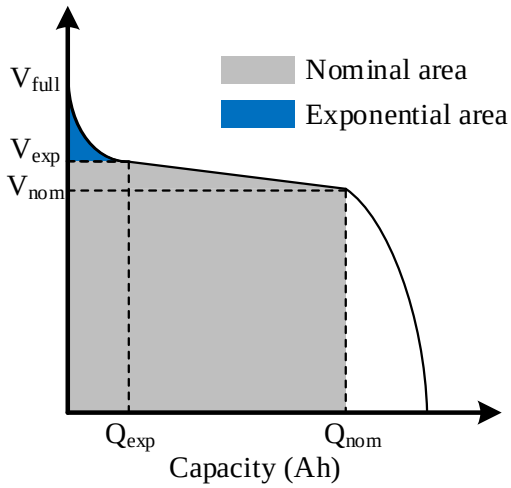

Figure 2: Battery charge and discharge curve. In this paper, 10 kWh battery is used. $V_{full} = 291\ V$, $V_{exp} = 270\ V$, $V_{full} = 250\ V$, $Q_{exp} = 1.96\ Ah$, $Q_{nom} = 36.17\ Ah$.

current (TC). CC charges the battery by keeping a constant charging current. The charging process will stop when the voltage reaches a preset value. However, to avoid overcharge, the current is required to set a small value. So this method is used in slow charge. In contrast to CC, CV charging begins at a constant voltage with a decreasing current. This method is usually used in less expensive EVs' chargers. However, since the voltage of each charging battery are different, CV charging may generate high current and damage battery when the voltage difference between battery and charger is significant. In TC charging, the charging current decreases proportionally to the rising voltage. This method is often used in low capacity battery and will not be considered in this paper.

Based on aforementioned analysis, a charging method includes the integration of CC and CV charging is adopt in this project. The charging process is named as CC/CV and is shown in Fig. 3 [10]. At the initial stage, the charging current is kept constant to avoid over-current. The charging will change to CV mode when the voltage reaches a preset value. At the CV mode, the battery is charged by a constant voltage with decreasing current. The most capacity of a battery is charged at CC mode, but the CV mode may take the same or longer time than CC.

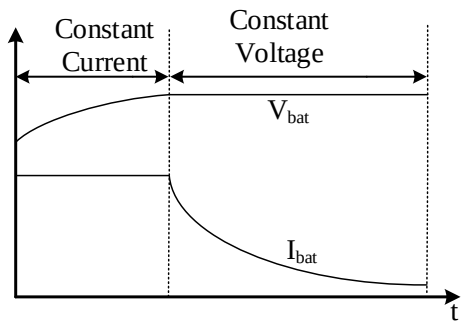

Figure 3: Illustration of CC/CV control. The parameters of the model are: Level 1 $V_{CV} = 262\ V$, $I_{CC} = 5\ A$; Level 2 $V_{CV} = 273\ V$, $I_{CC} = 40\ A$; Level 3 $V_{CV} = 279\ V$, $I_{CC} = 80\ A$;

The implementation of CC/CV is shown in Fig. 4. Two proportional integral (PI) controllers are used to ensure current and voltage as constant, respectively. The function of the selector is to switch CC or CV mode. In the beginning, the selector is connected to the current control mode to realize CC control. The charging voltage is compared with a preset value. The selector will turn to voltage control mode when the voltage reaches the preset value. The output of the control system is phase shift. The phase shift is the phase shift between DAB's ac voltages of two ends. In subsection 2.2, how phase shift can be realized and how it can influence power level will be explained.

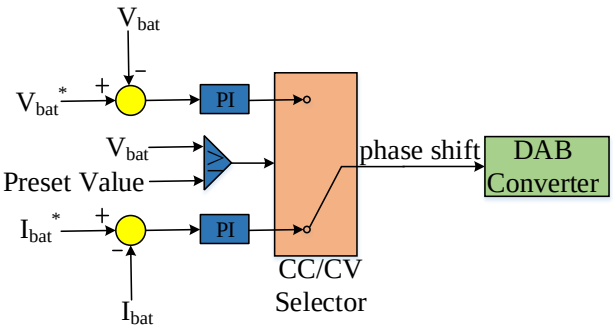

Figure 4: CC/CV charging structure, the connection of selector depends on battery voltage. The preset value is constant voltage.

2.2. Dual active bridge converter

Dual active bridge converter is widely used in the application of automobiles and renewable energy sources[11, 12]. This paper adopts the DAB converter to fulfill the requirement of regulating battery charging current and voltage.

The DAB structure is shown in Fig. 5. The DAB consists of two H-bridge converters. A high-frequency transformer is used to connect the converters. Both the two converters have the same switching frequency and duty-ratio (50%). The amount and direction of the power transfer can be changed by controlling the phase shift of the voltage on the two sides. The voltage phasors of the fundamental frequency on the two sides are denoted as V_1 and V_2. The phase shift of the two voltage is represented as angle θ, which is shown in Fig. 6.

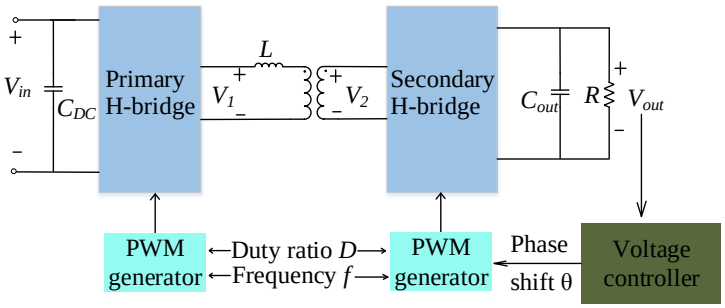

Figure 5: Structure of DAB converter, $f = 2\ kHz$, $D = 0.5$.

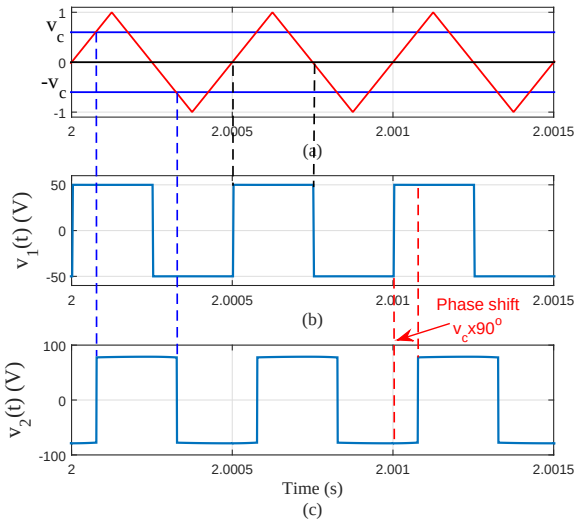

Figure 6: DAB converter control waveform and voltages: (a) v_c, $-v_c$ and 0 compared with a triangle waveform, (b) primary side voltage, (c) secondary side voltage.

The power transfer of the DAB can be expressed as:

$$P = \frac{V_1 V_2}{\omega L} \sin\theta \tag{2}$$

where L is the inductor in the primary side, ω is related to the switching frequency as $2\pi \times 2000\ rad/s$.

Assuming the output capacitor C_{out} ensures the output voltage V_{out} be a constant, if we consider only the fundamental component, then the RMS values of V_1 and V_2 can be written as:

$$\begin{aligned} V_1 &= \frac{4}{\pi}\frac{1}{\sqrt{2}}V_{in} \\ V_2 &= \frac{4}{\pi}\frac{1}{\sqrt{2}}V_{out} \end{aligned}$$

The power transfer can be expressed as (3).

$$P = \frac{V_1 V_2}{\omega L}\sin\theta = \frac{\frac{1}{2}(\frac{4}{\pi})^2 V_{in} V_{out}}{\omega L}\sin\theta \tag{3}$$

If all elements are ideal and there is no switching loss, the input power equals to the output power, shown in (4) and (5).

$$\frac{\frac{1}{2}(\frac{4}{\pi})^2 V_{in} V_{out}}{\omega L}\sin\theta = \frac{V_{out}^2}{R} \tag{4}$$

$$\Rightarrow V_{out} = \frac{\frac{1}{2}(\frac{4}{\pi})^2 R V_{in}}{\omega L}\sin\theta \tag{5}$$

where R is assumed as the load resistance.

The small signal model of V_{out} can be expressed as (6).

$$\Delta V_{out} = \underbrace{\frac{\frac{1}{2}(\frac{4}{\pi})^2 R V_{in}\cos\theta}{\omega L}}_{K_1} \cdot \Delta\theta \tag{6}$$

Since V_{in}, R, ω and L are all constants, then the output voltage V_{out} is proportional to phase shift θ.

$$\Delta V_{out} \propto \Delta\theta \tag{7}$$

Similarly, the current also can be expressed in small signal model as (8).

$$\Delta I_{out} = \underbrace{\frac{\frac{1}{2}(\frac{4}{\pi})^2 V_{in}\cos\theta}{\omega L}}_{K_2} \cdot \Delta\theta \tag{8}$$

This equation shows the output voltage or current can be controlled by adjusting the phase shift angle θ. The block diagram of the phase shift control model is shown in Fig. 7. To make V_{out} or I_{out} follow a reference value, the error is fed into a PI controller to generate phase shift. This phase shift can be realized by adjusting the control signal of the receiving end converter PWM generator, as explained in Fig. 6(a). If the reference control signal v_c is 0, the two blue lines will be aligned with the horizontal axis and 0 phase shift generated. If the control signal value is 1, the two blue lines will be located at the top and the bottom, which results in 90 degree phase shift. Phase shift is proportional to the control signal v_c.

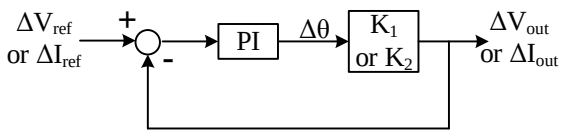

Figure 7: Diagram block of DAB converter. Input and output are in real value.

The Bode plots and step response of the DAB closed-loop output current control model are illustrated in Fig. 8. Different PI values are applied to compare their dynamic characteristics. In this model, the PI value $0.01 + \frac{0.1}{s}$ is chosen due to its fast dynamic performance.

2.3. PFC boost circuit

As Fig. 1 shows, a diode-based ac/dc converter is used to convert the ac voltage source to dc. However, the converter may generate non-sinusoidal currents thus results in low efficiency. Thus, a power factor correction (PFC) boost circuit is employed to achieve higher power factor or even unity power factor.

The PFC improves power factor (PF) by reshaping input current to be in phase with the input voltage[13, 14]. Fig. 9 demonstrates the impact of PFC by comparing the input voltage and current in the system with and without PFC. The current in the system with PFC is almost a sinusoidal waveform and has the same phase with the input voltage. In contrast, without PFC, the current shows the harmonics and phase shift with voltage.

The PFC circuit is shown in Fig. 10, the circuit includes two vital parameters: DC bus capacitor C_{DC} and inductor L_1. The two parameters determine the performance of the circuit. Thus, an appropriate design

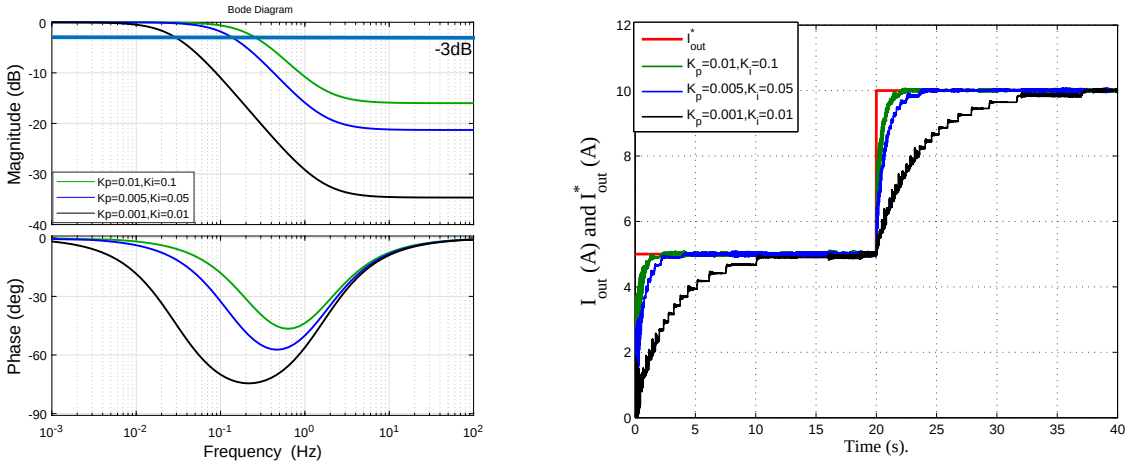

(a) (b)

Figure 8: The impact comparison of DAB PI controllers in Level 1 charger: (a) Bode plot, (b)step response. In Level 1 charger, $K_2 = 18.8$, when $k_p = 0.01$ and $k_i = 0.1$, the system has the largest bandwidth and fastest response time.

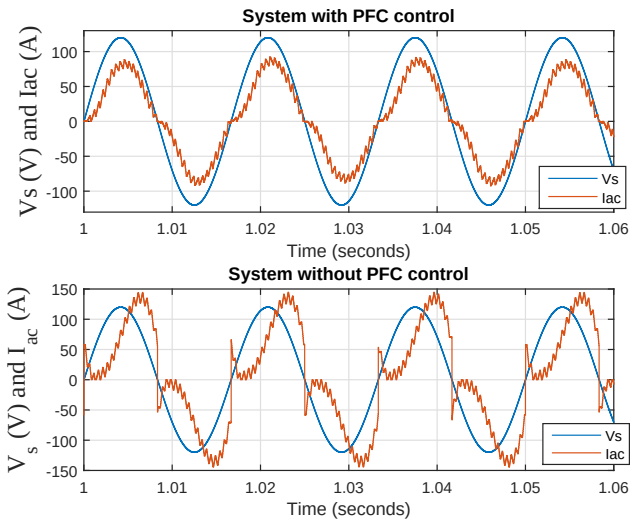

Figure 9: Comparison of boost converter performance with and without PFC control. The system without PFC control has a fixed duty ratio.

for the parameters is necessary. The values are deigned based on following analysis.

Assuming that the PFC has a unity power factor, the instantaneous active power of the charger is as follows.

$$p(t) = P + P\cos(2\omega t) \tag{9}$$

where ω is 377 rad/s and P is the active power.

The output capacitor ensures that the output voltage can be treated as a constant dc voltage. The

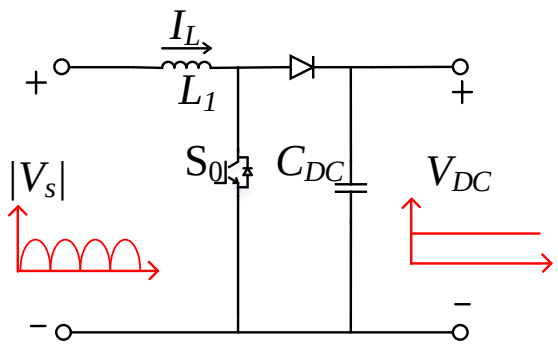

Figure 10: PFC circuit.

active power is consumed by load and the second frequency power ripple is expected to be absorbed by the capacitor. The output current is $I_{\text{out}} = \frac{P}{V_{\text{DC}}}$, and the capacitor current is calculated as (10).

$$i_c(t) = \frac{P\cos(2\omega t)}{V_{\text{DC}}} = I_{\text{out}}\cos(2\omega t). \tag{10}$$

Since the current through a capacitor is determined by $C\frac{dv_c}{dt}$, the voltage ripple can be found by integrating capacitor current as (11) shown.

$$v_{c2}(t) = \frac{1}{C_{\text{DC}}}\int i_c(t)dt = \frac{I_{\text{out}}}{2\omega C_{\text{DC}}}\sin(2\omega t). \tag{11}$$

Thus the peak-to-peak voltage ripple is presented by (12).

$$\Delta V_C = \frac{I_{\text{out}}}{2\pi f C_{\text{DC}}} \tag{12}$$

The battery voltage ranges 200 V to 400 V so the PFC circuit should support the maximum output voltage, 400 V[15]. According to Table. 1, the maximum power rating is 14.4 kW. So considering the maximum output voltage, the current is $\frac{14.4\,kW}{400\,\text{V}} = 36\ A$. If the peak-to-peak voltage ripple is less than 10 V, and the current is chosen as 36 A, then the capacitor is calculated as 9.5 mF.

The inductor current ripple can be found based on (13).

$$V_L = L\frac{di}{dt} \Rightarrow V_{\text{out}} - V_{\text{in}} = L\frac{\Delta i_L}{DT} \tag{13}$$

where D is duty ratio and T is switching period.

Since the PFC boost circuit is able to handle a wide range of output voltage, then the output is chosen as maximum value, 400 V, and the input is Level 1 input voltage, 120 V RMS single phase voltage. For a 120 V AC voltage, the mean value of the rectified voltage is 108 V. So the duty ratio is $D = \frac{V_{\text{out}} - V_{\text{in}}}{V_{\text{out}}} = 0.73$. The circuit is operated at a switching frequency of 2 kHz, and if 1 A current ripple is allowed, then the inductor needs to be 98 mH.

The PFC controller consists of two control loops: inner inductor current loop and outer DC bus voltage loop. Fig. 11 shows a PFC controller block [13]. The outer PI controller is utilized to ensure the DC bus voltage V_{DC} of the boost converter follow a fixed reference voltage. The output of the V_{DC} PI controller is

multiplied by the rectified sinusoidal voltage to generate a reference inductor current which is in the same phase with the rectified voltage. Similarly, the inner PI controller regulates the inner inductor current to follow the reference current. The inner PI controller generates the duty ratio of the PFC boost converter. Thus, the PFC controller is able to shape the current to be synchronized with voltage and regulate V_{DC}.

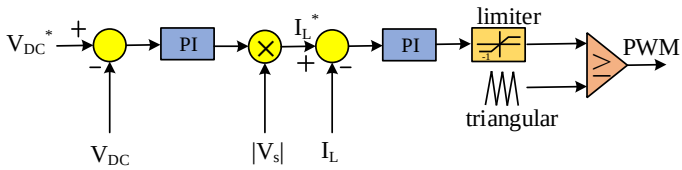

Figure 11: Block diagram of PFC control. The outer loop controller is $0.0005 + \frac{0.005}{s}$, inner loop controller is $0.01 + \frac{0.1}{s}$.

Fig. 12 shows the dynamic performance of this PFC. A step change to the PFC is applied by increasing the reference output voltage at $t = 4s$ from 200 V to 250 V and decreasing it at $t = 8s$ to 150 V. It can be observed that the duty ratio and inductor current also have an increase and decrease followed by reference voltage.

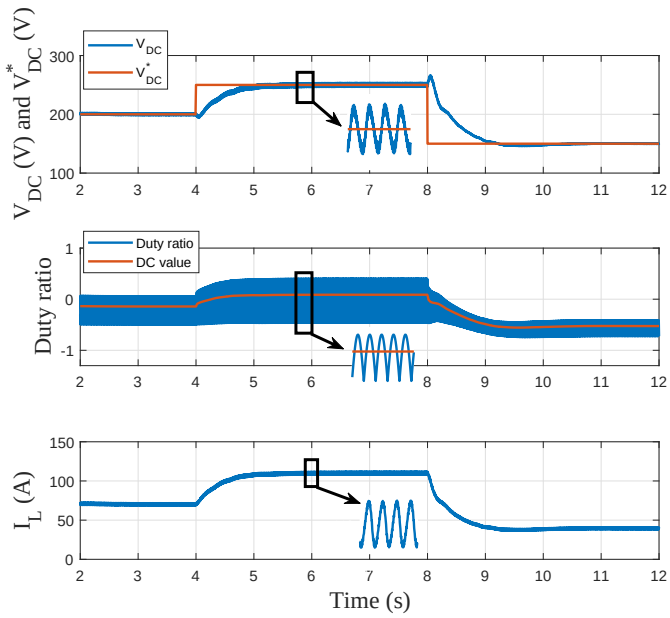

Figure 12: Step response of a PFC example.

3. Level 3 charging circuit topology

Since the Level 3 charging system uses three-phase voltage as power source, a three-phase converter is required. In this project, a bi-directional voltage source converter is adopted. This converter is controlled by a V_{DC}/Q controller which regulates the DC bus voltage and reactive power that receives from grid. A DAB bidirectional converter is followed. The DC bus voltage is the input of the DAB converter, which controls

the battery charging voltage or current using CC/CV. In addition, this charger is able to realize the vehicle to grid (V2G) service by controlling the power flow direction. The topology of Level 3 charger is shown in Fig. 13.

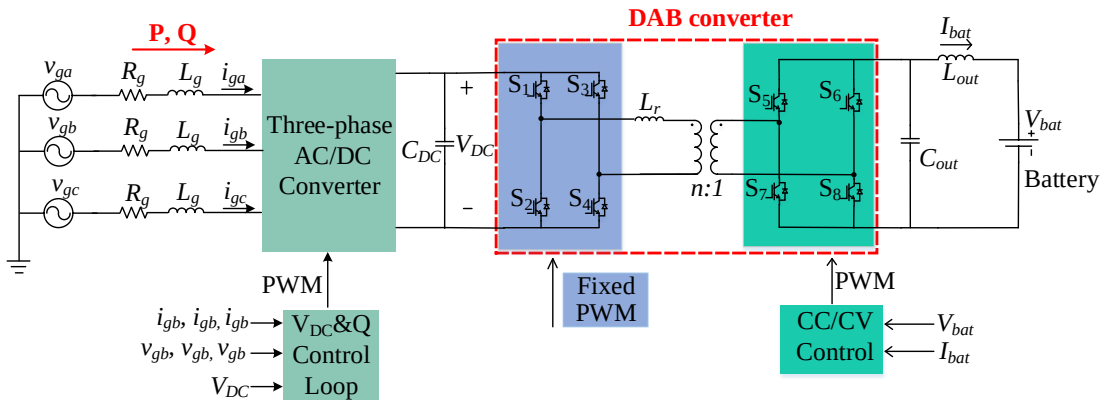

Figure 13: Topology of level-3 charging system, $R_g = 3\ m\Omega$, $L_g = 3\ mH$, $C_{DC} = 30\ mF$, $L_r = 0.13\ mH$, $f_{PWM} = 2\ kHz$, $L_{out} = 100\ mH$, $C_{out} = 0.1\ mF$, $n = 1$.

3.1. V_{DC}/Q controller

The V_{DC}/Q controller structure is shown in Fig. 14. The controller receives the measurements of DC bus voltage V_{DC} and reactive power Q from the grid. The two measurements are compared with their reference values. The differences are fed into two PI controllers and results in dq-axis current orders, which are converted into three-phase form by use of the angle of the input voltage space vector (θ). The grid voltage v_a, v_b and v_c are injected into a phase-locked-loop (PLL) to generate the angle (θ). The three-phase input current and voltage are converted into dq-variables based on a dq-frame with its d-axis aligned to the grid voltage. Real and reactive power absorbed by the EV from the grid are expressed as follows.

$$P = \frac{3}{2}(v_d i_d + v_q i_q) = \frac{3}{2} v_d i_d, \tag{14}$$

$$Q = \frac{3}{2}(v_q i_d - v_d i_q) = -\frac{3}{2} v_d i_q. \tag{15}$$

Note that the grid voltage is aligned to the d-axis. Hence $v_q = 0$. In addition, P can be adjusted by varying i_d while Q can be adjusted by varying i_q. Due to the negative linear relationship, reactive power control will be a positive feedback control, as shown in Fig. 14.

Three proportional and resonant (PR) controllers are utilized to control the three-phase converter. The input of the PR controller is the error between measured input current and its reference which is generated from dq/abc conversion. The PR controller generates converter voltage, which will be scaled to generate PWM waveform applied to the three-phase converter.

3.2. PR controller

Three PR controllers are used in the V_{DC}/Q control system. The function of a PR controller is to eliminate steady-state error at a designed frequency. In contrast, the PI controller can only realize the function at zero frequency.

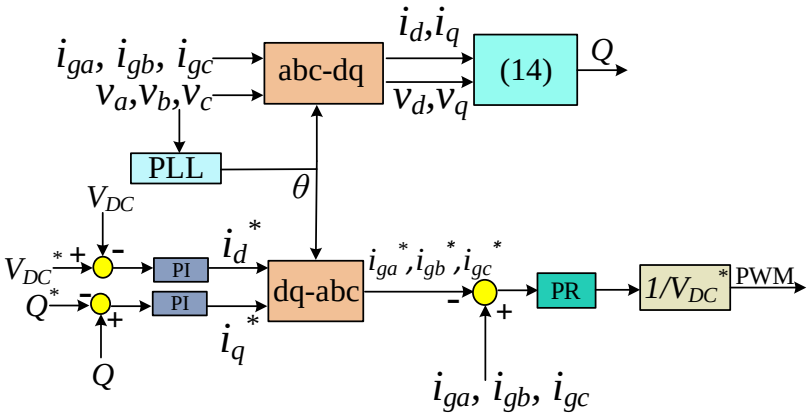

Figure 14: V_{DC}/Q control method applied to the three-phase converter, the V_{DC} PI controller is $0.1 + \frac{1}{s}$, reactive power controller is $0.01 + \frac{0.1}{s}$.

The transfer function of the PR controller is shown in :

$$G(s) = K_p + K_r \frac{2\omega_c s}{s^2 + 2\omega_c s + \omega^2} \tag{16}$$

where ω represents resonance frequency, ω_c is cutoff frequency, K_p is the proportional gain and K_r represents the resonant gain.

Note that the RT-Lab runs at discrete step size, so the PR controller should be modified to discrete time domain. Thus, the integrator $\frac{1}{s}$ is replaced by $\frac{T_s}{z-1}$, where T_s is the simulation step size, e.g., 50 μs. The block diagram of a discrete PR controller is shown in Fig. 15.

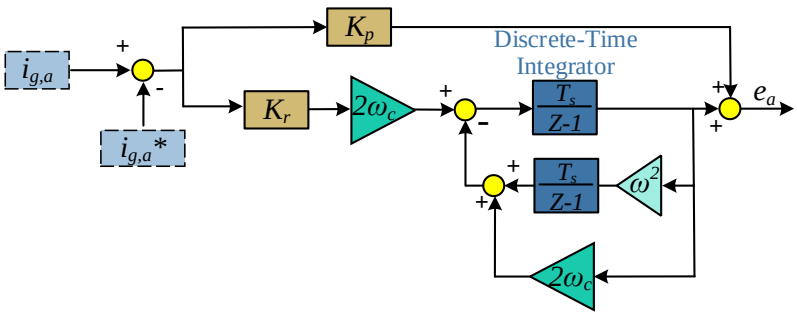

Figure 15: Structure of PR controller in phase a.

Considering the resonance frequency as 377 rad/s, both K_p and ω_c are fixed at 200. The Bode plot with varies K_r is shown in Fig. 16. As the Bode plot shows, the block gain is very large at the resonance frequency is 377 rad/s. So the PR controller is able to track a signal that frequency is 377 rad/s and the steady-state error will be eliminated. The K_r determines the width of the frequency bandwidth and dynamics. As illustrated in this Bode plot, a high K_r achieves a wider bandwidth compared to a low K_r. Thus, a high value is selected for K_r. In this model, PR controller is chosen as $200 + 1000\frac{400s}{s^2+400s+377^2}$.

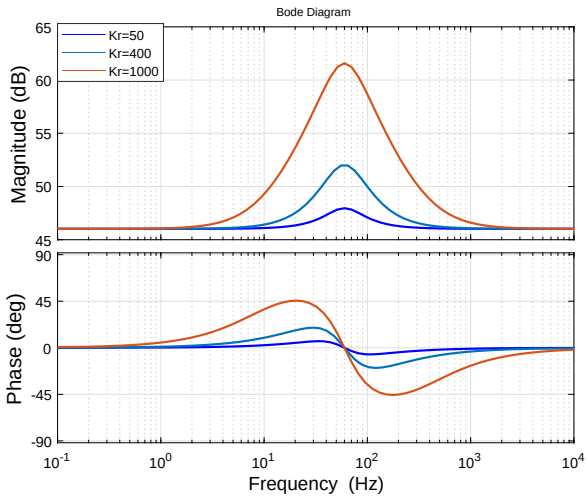

Figure 16: Bode plot of PR controller with varies K_r and $K_p = 200$, $\omega_c = 200$, $\omega = 2\pi \times 60$.

3.3. Phase locked loop

The function of a phase-locked-loop (PLL) is to synchronize the charging system to the grid. Three-phase grid voltage v_a, v_b, v_c are input to the PLL and then converted into dq-axis variables by using of the angle θ from PLL. The angle is the grid voltage space vector angle measured by PLL. A second-order PLL is adopted in this project, the diagram block is shown in Fig. 17 [16]. A PI controller is used to ensure v_q zero. The reference grid current i_d^* and i_q^* generated by DC bus voltage and reactive power will be converted to a-b-c form by using of the angle θ from PLL.

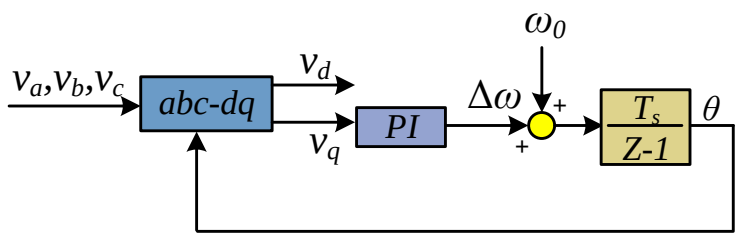

Figure 17: Block diagram of a PLL, the PI controller is $0.05 + \frac{1}{s}$. The input voltages are in real values.

A step change is applied to the controller as shown in Fig. 18. At $t = 4s$ DC bus reference voltage increases from 350 V to 400 V. At $t = 8s$ reactive power increases from 30 kVAR to 40 kVAR. The result shows that the DC bus voltage and reactive power can be well controlled.

4. Structure and performance of RT-Lab simulator

Considering the complicated model and long simulation time, real-time simulator RT-Lab is adopted. Firstly, the models are built in Matlab/SimPowerSystems. Then the models are converted to C code and implemented in RT-Lab. The RT-Lab simulates the power system model at the same rate as the physical time. Thus it offers much faster simulation speed.

A RT-Lab model is separated into three subsystems as master, slave and console subsystem. The master subsystem includes the computational and control part [17]. For example, the PFC control, CC/CV control,

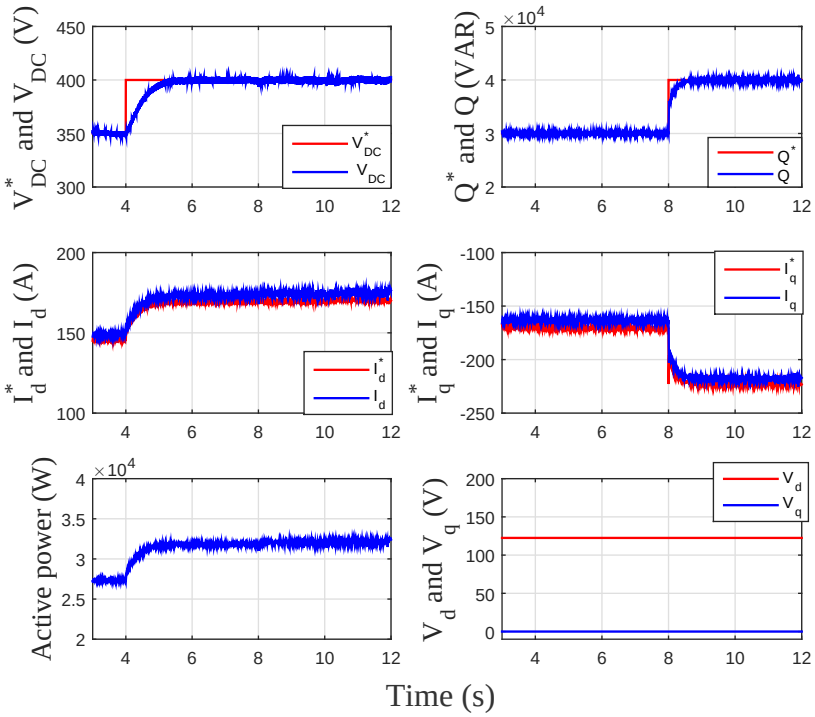

Figure 18: Step response of V_{DC}/Q control

and V_{DC}/Q control are assigned to the master subsystem. The slave subsystem consists of the circuit elements that include the voltage source, battery model, IGBTs, etc. The master and slave subsystem are located on different CPUs of the RT-Lab, so they are implemented in parallel to increase computation speed. The console subsystem is used to monitor the model while the model is executing. Users also can change the parameters of the model during simulation. It has to be mentioned that the console subsystem does not need devoted CPU.

The charging system real-time simulation modeling structure is shown in Fig. 19. The slave system includes the main circuit, where the measured parameters such as battery voltage and current, DC bus voltage are extracted and put into master subsystem. In the master subsystem, these parameters will be analyzed and control signals will be generated and sent to the main circuit.

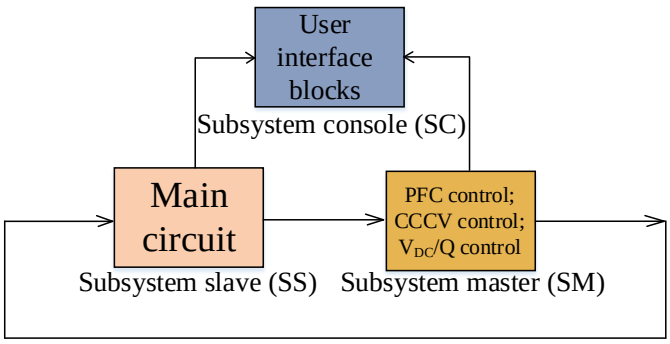

Figure 19: RT-Lab model structure.

In each simulate time step, the RT-Lab needs to complete three procedures: input, calculation and output. At the beginning, the RT-Lab reads the input data and then copes with these data based on functions. After processing these data, the results will be sent back to the model. The execution time of the three procedures should be less than the step size. Otherwise an error 'overrun' will happen in the model. The 'overrun' may cause the next step time omitting and thus data lost [18]. So the overrun should be avoided to make sure the accuracy of the model. If the three procedures take less time than the step size, the rest time is called idle time. The process of the simulation is shown in Fig. 20.

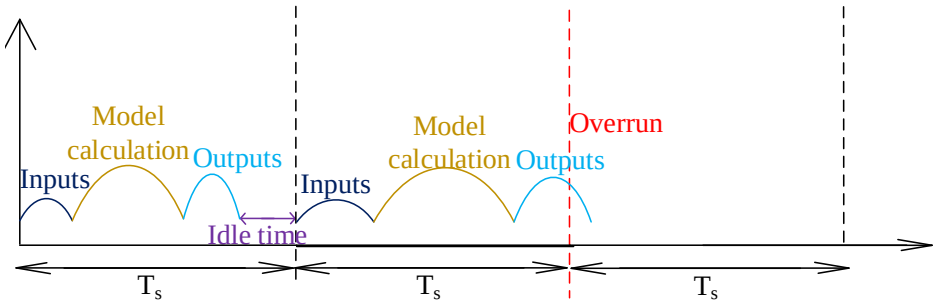

Figure 20: RT-Lab model time-step structure.

5. Simulation results

This section shows the real-time simulation results of proposed three-level charging systems in RT-Lab simulator. The battery used in the system has the power rating of 10 kWh and capacity is 40 Ah. The overall simulation shows the charging voltage, current, power and phase shift, DC bus voltage, PFC inductor current, reactive power and battery SOC comparison.

Figs. 21-22 present Level 1 charging process. At the beginning, the charging starts with a constant current, 5 A, while the voltage is increasing. The current will decrease when the voltage reaches the preset value, 262 V. The DC bus for Level 1 charging is 300 V. The results validate the CC/CV charging method. Figs. 23-24 show Level 2 charging simulation, which also includes two stages: CC and CV. At CC stage, the current is 40 A and charging turns to CV mode when the voltage is 272 V, and the DC bus voltage is also 300 V. In CV mode, with the charging power decreasing, the phase shift and inductor are also followed to decrease. Figs. 25-26 present Level 3 charging process. The constant current is 80 A and the constant voltage is 273 V. The DC bus voltage is 350 V and the reactive power keeps as 30 kVAR.

Fig. 27 shows the SOC comparison of the three-level charging system in the same time period. Level 3 charger is the fastest charging which increases the SOC from 10% to 82%. Level 2 charging increases the SOC from 10% to 48%. Level 1 charger is the slowest, and it only charges the battery to be 5% more in 25 minutes.

Based on the simulation waveforms, the numerical results are summarized in Table. 2. The charging currents, voltages and power ratings correspond to the SAE's standard. The estimate fully charging time means the time consuming to fully charge a 0% SOC battery to 100%.

In RT-Lab, Opmonitor block is used to record the model's procedures. Figs. 28 show the RT-Lab performance of three systems. Step sizes of all models are set as 20 μs, and no overrun occurs in simulation period, which indicates stable simulation condition.

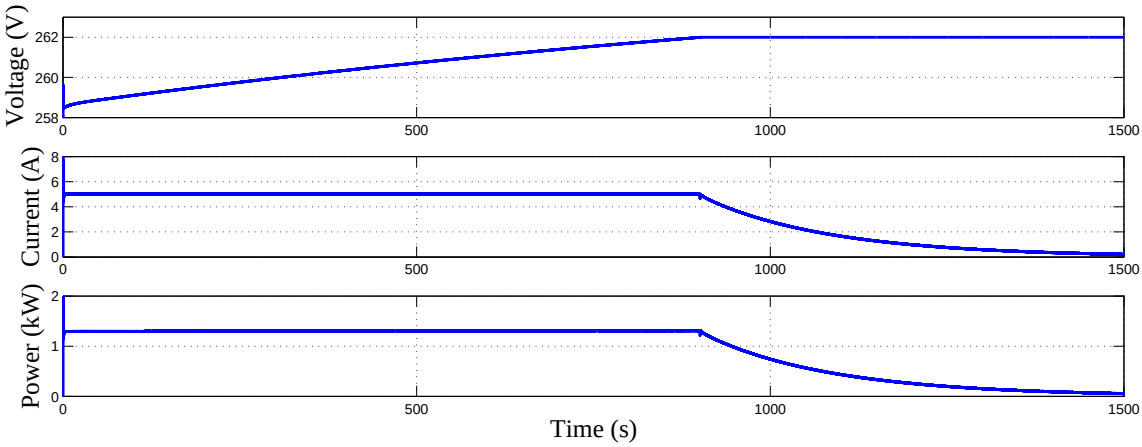

Figure 21: Current, voltage and charging power of Level 1 charging.

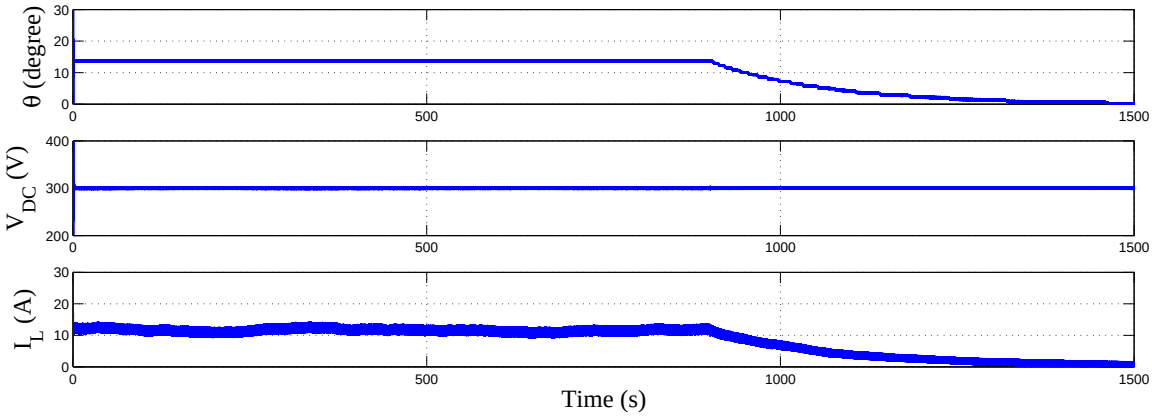

Figure 22: Phase shift angle, DC bus voltage and inductor current of Level 1 charging.

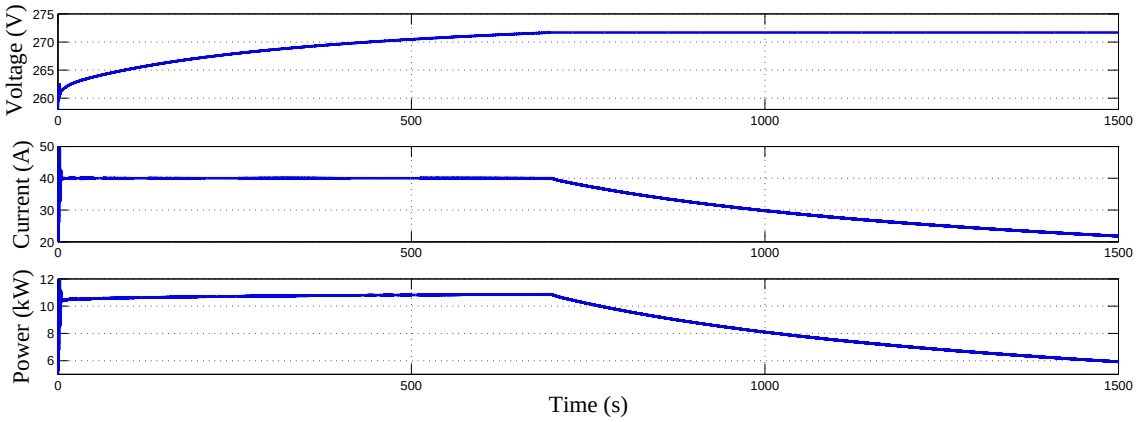

Figure 23: Current, voltage and charging power of Level 2 charging.

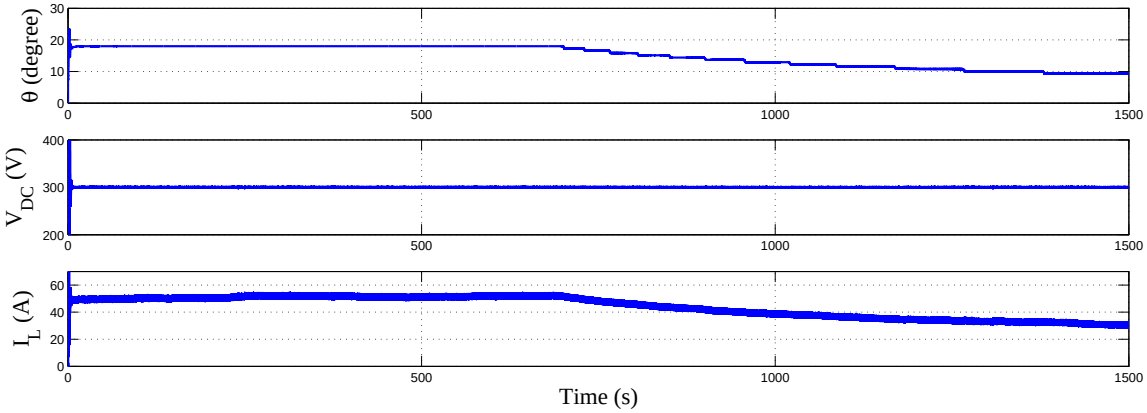

Figure 24: Phase shift angle, DC bus voltage and inductor current of Level 2 charging.

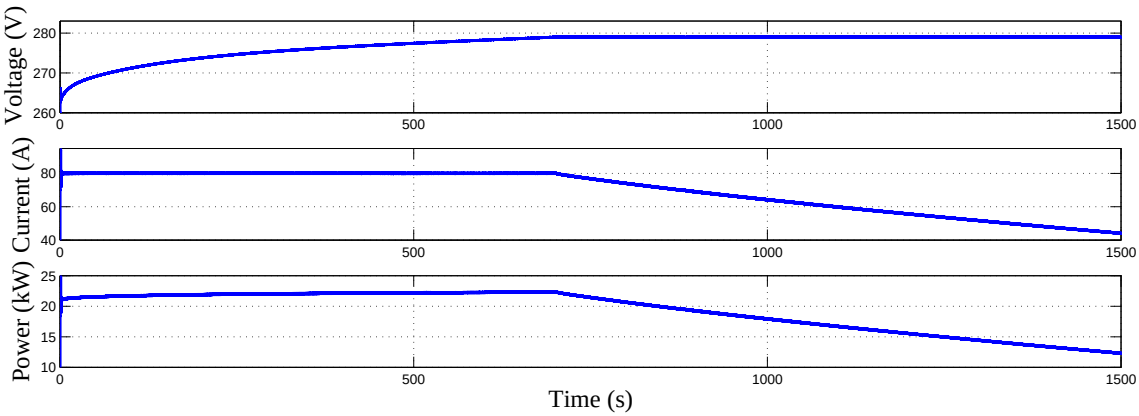

Figure 25: Current, voltage and charging power of Level 3 charging.

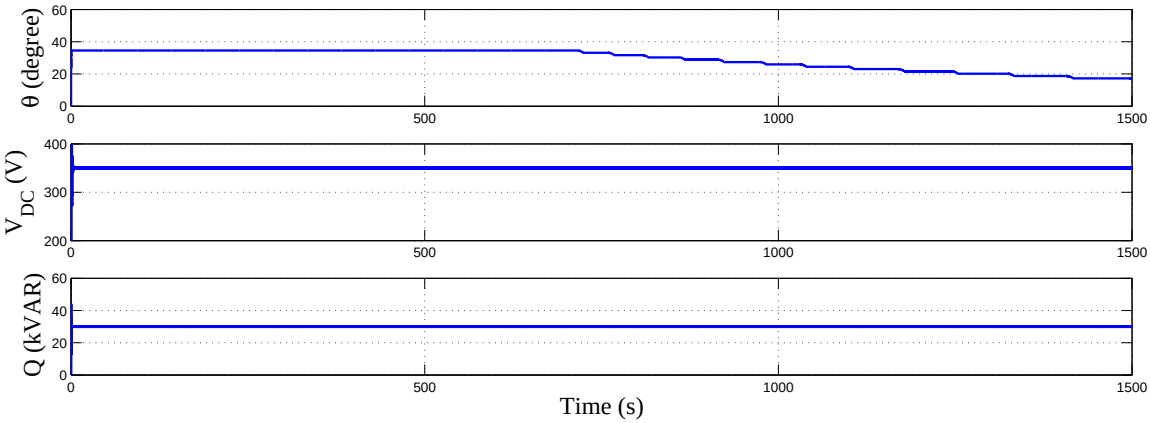

Figure 26: Phase shift angle, DC bus voltage and ractive power of Level 3 charging.

Table 2: Simulation analysis

	Level 1	Level 2	Level 3
Initial SOC	10%	10%	10%
Initial phase shift	12°	18°	33°
DC bus voltage	300 V	300 V	350 V
Charging power	1.31 kW	10.92 kW	22.32 kW
Constant current	5 A	40 A	80 A
Constant voltage	262 V	272 V	279 V
End SOC	14.3%	48.4%	82.3%
Estimated fully charging time	10 hours	1.1 hour	35 mins

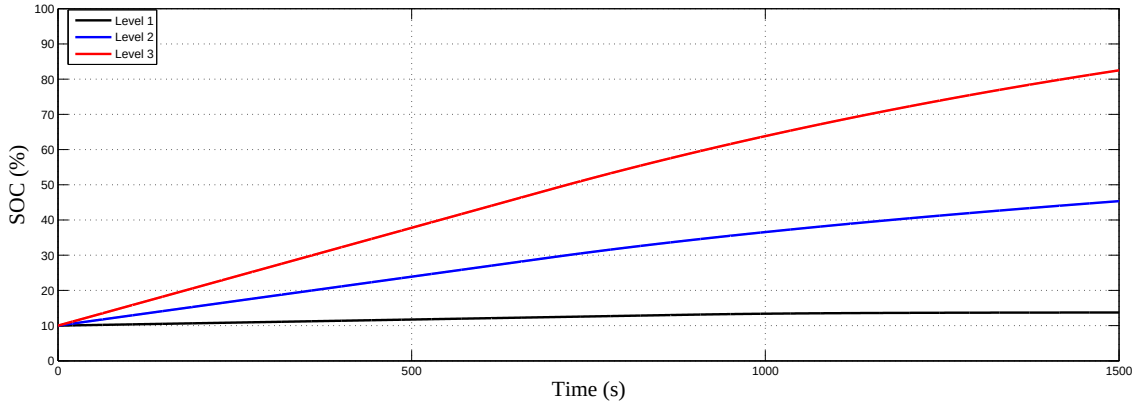

Figure 27: SOC comparison of three testbeds.

6. Conclusion

The paper presents the circuit topology, control and real-time simulation implementation of charging systems for EVs at three levels. Level 1 and Level 2 battery charging systems consist of a diode-based AC/DC converter, a PFC boost circuit, a DAB converter, a battery, and the related control systems. A PFC controller is employed to ensure a constant DC bus voltage and unity power factor. The CC/CV charging control is implemented the DAB converter. Level 3 charging system consists of a bi-directional three-phase AC/DC voltage source converter and a DAB converter. V_{DC}/Q control is employed on the AC/DC converter to regulate the DC bus voltage and reactive power. Simulations are implemented in RT-Lab simulator to demonstrate the charging processes of the charging system performance.

References

[1] U. S. energy information Administration, Monthly energy review (April 2018).
URL https://www.eia.gov/totalenergy/data/monthly/whatsnew.php

[2] J. Y. Yong, V. K. Ramachandaramurthy, K. M. Tan, N. Mithulananthan, A review on the state-of-the-art technologies of electric vehicle, its impacts and prospects, Renewable and Sustainable Energy Reviews 49 (2015) 365 – 385. doi:https://doi.org/10.1016/j.rser.2015.04.130.
URL http://www.sciencedirect.com/science/article/pii/S1364032115004001

[3] P. M. Menghal, A. J. Laxmi, Real time simulation: Recent progress amp; challenges, in: 2012 International Conference on Power, Signals, Controls and Computation, 2012, pp. 1–6. doi:10.1109/EPSCICON.2012.6175278.

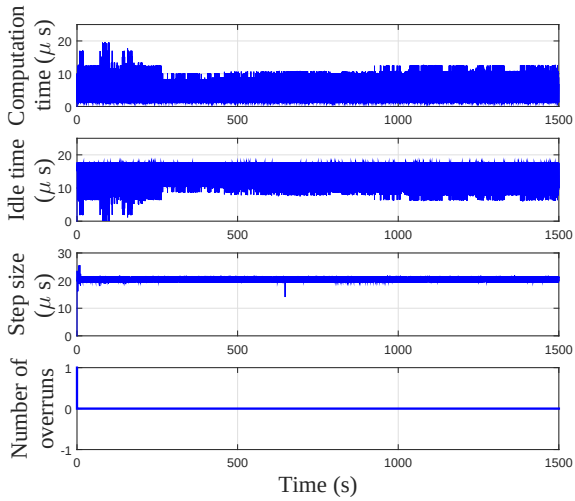

(a)

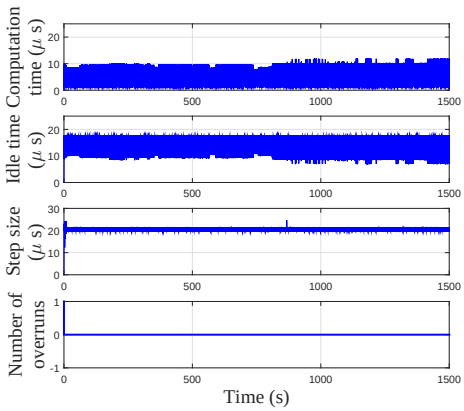

(b)

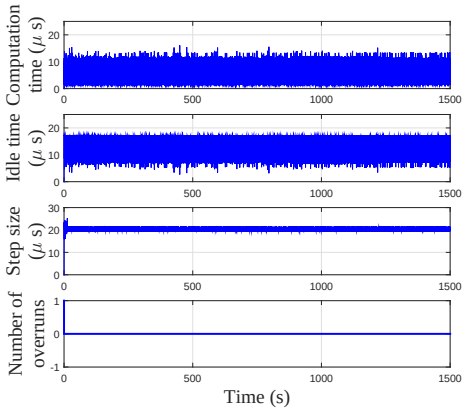

(c)

Figure 28: RT-Lab performance for: (a) Level 1 charging, (b) Level 2 charging, (c) Level 3 charging.

[4] L.-F. Pak, M. O. Faruque, X. Nie, V. Dinavahi, A versatile cluster-based real-time digital simulator for power engineering research, IEEE Transactions on Power Systems 21 (2) (2006) 455–465. doi:10.1109/TPWRS.2006.873414.

[5] S. Abourida, C. Dufour, J. Belanger, G. Murere, N. Lechevin, B. Yu, Real-time pc-based simulator of electric systems and drives, in: APEC. Seventeenth Annual IEEE Applied Power Electronics Conference and Exposition (Cat. No.02CH37335), Vol. 1, 2002, pp. 433–438 vol.1. doi:10.1109/APEC.2002.989281.

[6] C. Dufour, J. Belanger, A pc-based real-time parallel simulator of electric systems and drives, in: Parallel Computing in Electrical Engineering, 2004. International Conference on, 2004, pp. 105–113. doi:10.1109/PCEE.2004.8.

[7] M. Yilmaz, P. T. Krein, Review of battery charger topologies, charging power levels, and infrastructure for plug-in electric and hybrid vehicles, IEEE Transactions on Power Electronics 28 (5) (2013) 2151–2169. doi:10.1109/TPEL.2012.2212917.

[8] O. Tremblay, L.-A. Dessaint, Experimental validation of a battery dynamic model for ev applications, World Electric Vehicle Journal 3 (1) (2009) 1–10.

[9] C. H. Dharmakeerthi, N. Mithulananthan, T. K. Saha, Modeling and planning of ev fast charging station in power grid, in: 2012 IEEE Power and Energy Society General Meeting, 2012, pp. 1–8. doi:10.1109/PESGM.2012.6345008.

[10] A. Tazay, Z. Miao, Control of a three-phase hybrid converter for a pv charging station, IEEE Transactions on Energy Conversiondoi:10.1109/TEC.2018.2812181.

[11] W. Song, B. Lehman, Dual-bridge dc-dc converter: a new topology characterized with no deadtime operation, IEEE Transactions on Power Electronics 19 (1) (2004) 94–103. doi:10.1109/TPEL.2003.820600.

[12] M.-T. Tsai, C.-L. Chu, Y.-J. Yang, D.-J. Wu, Design of a dual active bridge dc-dc converter for photovoltaic system application, ICIC express letters. Part B, Applications : an international journal of research and surveys 7 (2016) 1805–1812.

[13] C. Zhou, R. B. Ridley, F. C. Lee, Design and analysis of a hysteretic boost power factor correction circuit, in: 21st Annual IEEE Conference on Power Electronics Specialists, 1990, pp. 800–807. doi:10.1109/PESC.1990.131271.

[14] S. Lee, Effects of input power factor correction on variable speed drive systems, Ph.D. thesis, Virginia Tech (1999).

[15] P. T. Krein, Elements of power electronics, Vol. 126, Oxford University Press New York, 1998.

[16] L. Fan, Control and Dynamics in Power Systems and Microgrids, CRC Press, 2017.

[17] S. S. Noureen, V. Roy, S. B. Bayne, An overall study of a real-time simulator and application of RT-LAB using MATLAB simpowersystems, in: 2017 IEEE Green Energy and Smart Systems Conference (IGESSC), 2017, pp. 1–5. doi:10.1109/IGESC.2017.8283453.

[18] M. D. O. Faruque, T. Strasser, G. Lauss, V. Jalili-Marandi, P. Forsyth, C. Dufour, V. Dinavahi, A. Monti, P. Kotsampopoulos, J. A. Martinez, K. Strunz, M. Saeedifard, X. Wang, D. Shearer, M. Paolone, Real-time simulation technologies for power systems design, testing, and analysis, IEEE Power and Energy Technology Systems Journal 2 (2) (2015) 63–73. doi:10.1109/JPETS.2015.2427370.